THE ASTROPHYSICAL JOURNAL, 496:538–549, 1998 March 20
© 1998. The American Astronomical Society. All rights reserved. Printed in U.S.A.

IN-FLIGHT PERFORMANCE OF THE HIGH ENERGY X-RAY TIMING EXPERIMENT ON THE *ROSSI X-RAY TIMING EXPLORER*

R. E. ROTHSCHILD, P. R. BLANCO, D. E. GRUBER, W. A. HEINDL, D. R. MACDONALD, D. C. MARSDEN, M. R. PELLING, AND L. R. WAYNE
Center for Astrophysics and Space Sciences 0424, University of California at San Diego, La Jolla, CA 92093-0424

AND

P. L. HINK
Department of Physics, Washington University, St. Louis, MO 63130
Received 1997 August 19; accepted 1997 October 28

ABSTRACT

The High Energy X-Ray Timing Experiment (HEXTE) is one of three scientific instruments aboard the *Rossi X-Ray Timing Explorer* (*RXTE*), which was launched on 1995 December 30. *RXTE* performs timing and spectral studies of bright X-ray sources to determine the physical parameters of these systems. The HEXTE consists of two independent clusters of detectors, each cluster containing four NaI(Tl)/CsI(Na) phoswich scintillation counters sharing a common 1° FWHM field of view. The field of view of each cluster is switched on and off source to provide near real-time background measurements. The net open area of the eight detectors is 1600 cm^2, and each detector covers the energy range 15–250 keV with an average energy resolution of 15.4% at 60 keV. The in-flight performance of the HEXTE is described, the light curve and spectrum of the Crab Nebula/pulsar is given, and the 15–240 keV spectrum of the weak source, active galaxy MCG +8-11-11 is presented to demonstrate the weak source spectral capabilities of HEXTE.

Subject headings: instrumentation: detectors — space vehicles — telescopes — X-rays: general

1. INTRODUCTION

The High Energy X-Ray Timing Experiment (HEXTE) is one of three scientific instruments aboard the *Rossi X-Ray Timing Explorer* (*RXTE*) (see Fig. 1). The other instruments are the proportional counter array (PCA; Jahoda et al. 1996) and the all-sky monitor (ASM; Levine et al. 1996). The PCA and HEXTE are coaligned to provide 2–250 keV observations of individual sources, and the ASM independently monitors the ~100 brightest 2–12 keV sources in the sky (Swank et al. 1995). The HEXTE is the latest in a long-term program of hard X-ray instrumentation development for observational high-energy astrophysics that has included the UCSD Cosmic X-Ray Telescope on *OSO 7* and the A-4 Hard X-Ray and Low Energy Gamma-Ray Experiment on *HEAO 1*. The successful launch of *RXTE* on a Delta II expendable launch vehicle occurred at 13:47 UT on 1995 December 30. The first month of operations was devoted to in-orbit checkout (IOC), the results of which are described here.

2. INSTRUMENT DESCRIPTION

The HEXTE consists of two independent clusters of detectors. Each cluster contains four NaI(Tl)/CsI(Na) phoswich scintillation counters collimated by a lead honeycomb. All eight collimators are coaligned on source to give both clusters a 1° FWHM field of view. The net open area of the eight detectors is ~1600 cm^2, and each detector covers the energy range 15–250 keV with an average energy resolution of 15.4% FWHM at 60 keV. The cluster organization for the HEXTE instrument permits effective immunity to systematic background variations through the use of continuous gain control, chopping of the source signal, and anticoincidence shielding of charged particle events. The system requires about 45 W, exclusive of heater power, weighs about 400 kg, and utilizes 5 kbyte s^{-1} of telemetry on the average. Table 1 summarizes the HEXTE instrument characteristics.

The energy, time of arrival, and pulse shape associated with each detected photon are measured and digitized. For sources weaker than the Crab Nebula, all of this information may be telemetered to the ground. The maximum anticipated event rate for the brightest sources, however, does not allow all of this information to be transmitted, as each HEXTE cluster's data rate is limited to 23,000 bits s^{-1}. Thus, the on-board data processor permits, on command, the selection of any desired subset of each event's data to be telemetered. For very bright sources the processor has two binned analysis modes to permit considerable flexibility in data formatting and compression in order to achieve the timing and energy resolution requirements for source observations consistent with efficient data recovery.

The HEXTE instrument is sensitive to X-ray fluxes on timescales from milliseconds to days, limited only by the telemetry and the source intensity. HEXTE is capable of measuring a typical, weak (~1 mcrab) X-ray source to 100 keV or greater in 10^5 live seconds, i.e., it has a 3 σ sensitivity of 10^{-6} photons cm^{-2} s^{-1} keV^{-1} in a 20 keV band at 100 keV.

2.1. *X-Ray Detectors*

The primary HEXTE detection elements are eight 18.3 cm diameter by 0.3 cm thick NaI(Tl) scintillation crystals, each of which is optically coupled to a single 5 inch (12.7 cm) photomultiplier tube through an intervening 5.69 cm thick CsI(Na) shield crystal and 0.64 cm thick quartz window, as shown in Figure 2. The rear of the CsI(Na) crystal is tapered to match the photomultiplier tube's photocathode diameter (typically 11.4 cm). The CsI(Na) crystal provides uniform collection of primary NaI(Tl) crystal scintillation light and active anticoincidence shielding, both from X-ray events not originating in the look

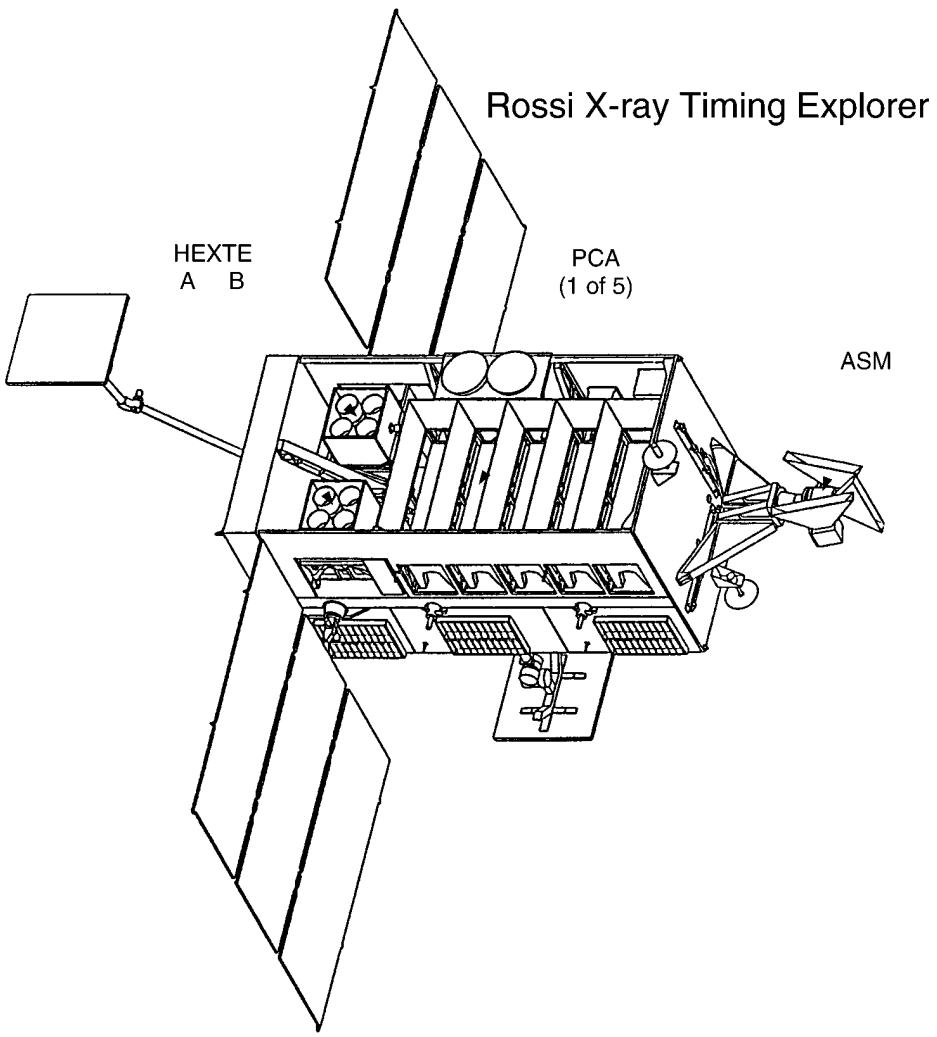

FIG. 1.—*RXTE* spacecraft viewed from above to reveal the scientific instruments. The five PCA proportional counters and the two HEXTE clusters are shown in relation to the rest of the spacecraft components, such as the two high gain antennae for communications with the ground via the tracking and data relay satellite system, the two solar-power arrays that can rotate to face the Sun, and the ASM on the end with clearance to view the sky.

direction, and from events with partial energy loss in the NaI(Tl).

The scintillation pulses generated within the two crystal media exhibit differing characteristic decay times, 0.25 μs in NaI(Tl) and 0.63 μs in CsI(Na). Signals from the photomultiplier tube are pulse-shape analyzed to distinguish pure NaI(Tl) energy losses from events containing some proportion of the slower component indicating an energy loss in the CsI(Na) shield crystal. Rejected events can be either charged particles that trigger both crystals or X-rays that leave partial energy in the NaI(Tl) and CsI(Na) crystals.

TABLE 1

HEXTE INSTRUMENT CHARACTERISTICS

Characteristic	Value
Energy range (keV)	15–250
Energy resolution at 60 keV	<17%
Time resolution (μs)	7.6
Field of view	1° FWHM hexagonal
Detector material	NaI(Tl), CsI(Na)
Net detector area (cm^2)	1600
Detection sensitivity in 10^5 s, 3 σ (photons cm^{-2} s^{-1} keV^{-1} at 100 keV)	10^{-6}
Gain control stability	0.3%
Source/background dwell time (s)	16–128
Calibration source	^{241}Am (17 and 60 keV)
Detector operating temperature	17°–19°C
Weight (kg)	400
Operational power (W)	45
Average telemetry rate (bits s^{-1})	5000

The crystals are contained in an opaque, hermetically sealed housing to prevent degradation of the NaI(Tl) by water vapor before launch and to shield the photomultiplier tube from stray light. The housing incorporates a 0.051 cm thick beryllium X-ray entrance window to provide a light seal with minimal low-energy absorption of incident X-rays. The crystals are wrapped in teflon sheet, 0.025 cm thick, and are highly polished to provide uniform light collection by the photomultiplier tube, thereby maximizing energy resolution.

The photomultiplier tube and its attendant high voltage divider network (bleeder string), coupling elements, and connectors are encased in silicone elastomer, and the entire potted assembly is contained within a metallic housing that acts as a magnetic shield to suppress modulation of the photomultiplier tube gain as the external magnetic field vector varies around the orbit (Rothschild, Pelling, & Hink 1991).

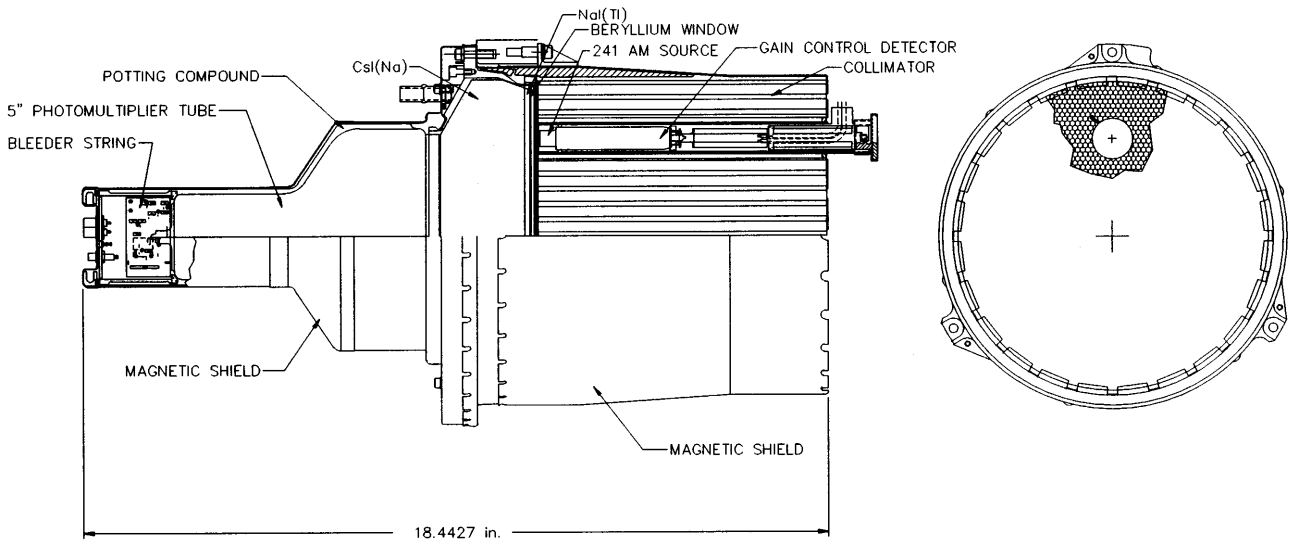

FIG. 2.—HEXTE detector module, consisting of photomultiplier tube, scintillation crystals, and collimator assemblies. The collimator assembly also contains the gain control photomultiplier and ^{241}Am doped plastic scintillator assembly. The upper half of the side view on the left is a cutaway revealing the inner elements of the module, while the lower half shows the magnetic shield housing that encases the entire module. The front view on the right gives the placement of the automatic gain control assembly in the collimator and shows a fraction of the collimator honeycomb.

2.2. *Particle Detectors*

Each HEXTE cluster includes three particle detection systems: (1) a set of cosmic-ray particle anticoincidence shield detectors, (2) an alpha particle coincidence detector for each phoswich for gain control and calibration, and (3) a single trapped radiation particle detector. The anticoincidence shield system consists of four flat 0.64 cm thick plastic scintillator modules configured in a four-sided box around the X-ray detectors. The shields provide a prompt anticoincidence signal for background events that are generated by energetic particle interactions occurring in the external mass of the instrument and satellite (Hink et al. 1991). The shields and the CsI(Na) of the phoswich detectors are sensitive to minimum ionizing particles from 95% of 4π sr.

Each phoswich detector module has an ^{241}Am calibration X-ray source mounted in the collimator immediately above its entrance window and viewed by a separate $\frac{1}{2}$ inch (1.27 cm) photomultiplier tube (see Fig. 2). The calibration module provides continuous feedback to the automatic gain control subsystem (Pelling et al. 1991), and calibration spectra (Fig. 3) are included in the flight telemetry. Gain control is effected by varying the pulse-height analyzer (PHA) gain twice per second in a feedback loop to keep the ^{241}Am 59.5 keV line at a constant pulse height. In-orbit performance shows that the line centroids are stable to better than 0.02 PHA channels on a 1 day timescale, where one channel is approximately 1 keV.

The single particle monitor detector in each cluster is a 1.27 cm diameter by 1.27 cm thick cylinder of plastic scintillator viewed by a $\frac{1}{2}$ inch photomultiplier tube. The aluminum housing provides a threshold energy of $\sim$0.5 MeV for electrons. The particle monitors are used to measure the ambient particle flux and safeguard the detector systems as they pass through the trapped radiation belts of the South Atlantic Anomaly (SAA). Safeguarding is accomplished automatically by reducing the photomultiplier bias voltages by a factor of 4 during times of high particle flux, thus limiting the anode and dynode currents to avoid fatigue effects. The high voltage levels automatically return when the particle monitor rate drops to a safe level.

2.3. *Source Beam Switching*

The HEXTE cluster rocking subsystem moves the viewing direction of the detector arrays between on source and off source in order to obtain a near real-time estimate of the instrument background. The nominal angular offset is 1°.5 on either side of the on-source position, with the option of increasing the offset to 3°.0 and/or rocking to only one side in cases where there is a known confusing source in a background field of view. Since the rocking axes of the two clusters are orthogonal to each other, four background regions are nominally sampled around a given source position. Data acquisition is inhibited during the 2 s transitions between on- and off-source positions, and the modulation of the two clusters is phased such that one cluster is always viewing on source. The beam switching cycle consists of dwelling at the on-source position for 16, 32, 64, or 128 s,

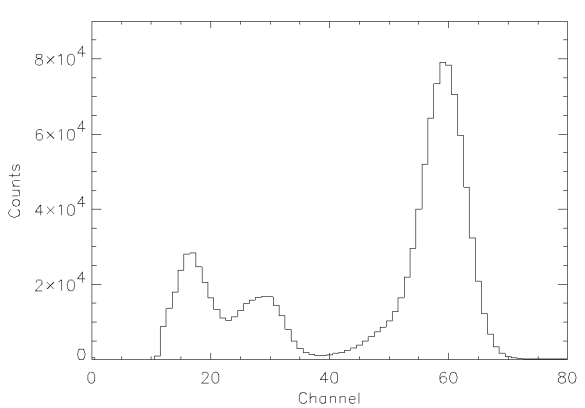

FIG. 3.—Calibration histogram of the HEXTE ^{241}Am gain control source. The data were accumulated over one day on 1997 January 10. The 60 keV gamma-ray line, the complex of Np L de-excitation lines around 17 keV, and the K-escape lines near 30 keV are evident. Each channel corresponds to approximately 1 keV.

moving to an off-source position, dwelling there for the same amount of time as on source (less the 4 s of transit time), moving back to the on-source position, and repeating for motion to the other off-source position. This cycle is repeated throughout the observation.

2.4. *HEXTE Electronics*

An 80C286 microprocessor running at 4.915 MHz is used to control each cluster and process its output data. Redundant interfaces are provided from each cluster to the spacecraft instrument power supply and distribution unit (IPSDU) and 1773 fiber-optic command and telemetry busses. The IPSDU also provides the conditioned and converted low voltage power to the cluster and interfaces to the instrument rocking, thermal control, and gain control subsystems. The electronics on each cluster exchange SAA detection and burst detection signals with the other, and, in the case of burst detection, exchange such signals with the PCA's data processor, known as the experiment data system (EDS).

2.5. *Data Processing/Telemetry Formatting*

In-flight programmable logic is used to control data selection on an event-by-event basis. Data for each event that passes the selection criteria are combined with other subsystem indicators and collected to form a 56 bit event code. This event code is then passed on to either the automatic gain control/calibration subsystem or the science processing/telemetry formatting process. The default data selection criteria are for the event energy loss to be within the HEXTE energy range, the event pulse shape to be that of pure NaI with no contribution from CsI, no recent (within 2.5 ms) large energy loss (>20 MeV), and no anticoincidence shield pulse present. This provides efficient data recovery for most observations by measuring the energy loss for only NaI(Tl) events. The HEXTE energy range is determined by the settings of the electronic pulse-height discriminators. The lower level discriminator is commandable between 5 and 50 keV, and in practice the default value is 12 keV. The upper level discriminator is fixed at 250 keV. System noise causes these discriminator edges to be imperfect, and the nonzero energy resolution results in some loss of events at the energy extremes. Consequently, data analysis is recommended to be in the 15–250 keV range.

Two standard mode data products are generated within HEXTE every 16 s. The purpose of these "archive" modes is to provide a basic temporal and spectral record of every source observed that is independent of the scientific mode chosen by the guest observer. The archive histogram mode produces a pseudologarithmically compressed 64 channel pulse-height histogram for each phoswich every 16 s. The archive multiscalar mode produces four light curves from the sum of all four phoswiches in a cluster with 1 s temporal resolution. The four light curves represent the approximate energy ranges of 15–29, 30–61, 62–125, and 126–250 keV. A measurement of the live time for each phoswich for each 16 s instrument data frame (IDF) is included with the standard mode data.

HEXTE science processing in each cluster can be configured to produce one of three modes at any given time: (1) event list mode, (2) histogram bin mode, or (3) multiscalar mode. The event list mode is an event-by-event list of a commandable subset of the event code for each photon detected. Any combination of the 7 bytes comprising the event code may be selected for inclusion in telemetry. Subsequent ground analysis is able to generate light curves and/or spectra, depending upon the event code bytes selected. The histogram bin mode produces a pulse-height histogram for each detector, or, alternatively, for the sum of all four detectors in a cluster. The histograms can be tailored to each observation by choice of the number of histograms per IDF, the number of pulse-height bins, the count capacity of each bin, and the full scale pulse-height channel value of each histogram. The multiscalar bin mode produces up to eight light curves, contiguous in energy with channel boundaries fully selectable, with commandable time sampling from 0.5 ms to 1 s, for either each detector or the sum of all four. A ninth light curve is available to accumulate the lost events (i.e., otherwise valid events that were not pulse-height analyzed because the analyzer was busy with a previous event) on the same timescale as the other light curves.

A fourth mode, burst list, can be enabled by command to run in parallel with any of the three basic science modes. This mode takes a "snapshot" of the data from a bright source at the highest spectral and temporal resolution for later transmission. The burst list mode buffers 4 bytes of the event code from each event in a circular buffer containing 25,600 events. Upon initiation by a burst trigger, the buffer accumulates a software-commandable number of posttrigger events, then freezes its contents and awaits a command to download its contents in place of the normal science data. Dead-time data are accumulated once each second for the first 48 s after the burst trigger and are included in the burst list buffer. A burst trigger can be generated by any of four sources: a serial digital ground command, a trigger received from the EDS electronics, a trigger received from the other cluster, or an internally calculated burst trigger. The internal burst trigger is issued upon detection of an increase in the recent average event rate exceeding a commandable threshold.

3. INSTRUMENT PERFORMANCE

Two anomalies have occurred that affect HEXTE performance: (1) the pulse-height analyzer of one detector has failed, and (2) the system for measuring dead time within the instrument does not properly register dead time after large energy losses in the crystals. On 1996 March 6 the pulse-height analyzer for the third phoswich in cluster B stopped digitizing pulse heights. The most probable cause was the failure of a single element, such as an operational amplifier or solder connection. Rates from this detector remain nominal, but energy information and the gain control function are lost.

During analysis of IOC data, it was realized that the analog circuitry that processes pulse-shape information for individual X-ray events was paralyzed after large energy losses for times substantially longer than anticipated. Since this system is required to identify NaI energy losses for subsequent pulse-height analysis, the consequence of this problem is to have the system reject otherwise valid events during the "recovery" period without incrementing the internal dead-time counters as intended. Consequently, the hardware dead time associated with a large energy loss was increased from 0.3 to 2.5 ms to minimize this effect. In addition, the remaining unmeasured dead time has been modeled using parameters associated with the more than 20 MeV extreme upper level discriminator rate (XULD) and with the more than 250 keV upper level discriminator rate

TABLE 2

HEXTE PHOSWICH ENERGY RESOLUTION

Phoswich	$\Delta E/E$ at 60 keV	Phoswich	$\Delta E/E$ at 60 keV
Cluster A, P0	0.1426	Cluster B, P0	0.1523
P1	0.1639	P1	0.1676
P2	0.1570	P2	0.1654
P3	0.1404	P3	0.1458

(ULD). These two parameters were determined for each detector by requiring the flux from the Crab Nebula to be constant on a 16 s timescale. Based upon observations of the Crab Nebula/pulsar spectrum (see below) the dead time appears to be mostly energy independent and only the normalization of measured fluxes is affected. The total mean HEXTE corrected dead time averages about 40%.

The average energy resolution of the eight detectors was seen to increase slightly in orbit from the prelaunch average of 14.8% to 15.4% at 60 keV (Hink, Pelling, & Rothschild 1992). This increase is believed to be due to presence of additional "noise" in the scintillation light signal due to long-lived decay states that are excited by large cosmic-ray energy loss events in the NaI(Tl) crystals. The energy resolution of the phoswiches is given in Table 2, and shown as a function of energy in Figure 4. The HEXTE effective area as a function of energy is shown in Figure 5. This incorporates the estimated physical open area per detector and the energy-dependent response of the detector as determined by Monte Carlo simulation. The simulation reproduces data taken before launch using both radioactive sources and monochromatic X-rays at the Brookhaven National Synchrotron Light Source (Wayne et al. 1998). It also includes the effects of K-escape X-rays, Compton scattering, the nonlinearity of light output of NaI(Tl), and pulse-shape discrimination versus energy.

3.1. *Instrument Background*

Figure 6 shows the HEXTE background from 7.5 hr of observing blank fields on 1996 January 15, during the in-orbit checkout phase of the mission. The background is dominated by internal activation effects, with less than 5% of the total due to the cosmic X-ray background transmitted by the 1° aperture of the collimators. Prominent background lines due to activation are seen at 30 keV (the K lines from the Te daughters of various iodine decays), 55 keV (due to ^{121}I decay), and near 190 keV (due to ^{123}I). K-escape lines from the 190 keV complex are also evident at $\sim$160 keV. The blend of K lines from fluorescence of lead in the collimator by charged particles and cosmic X-rays is prominent from 60 to 90 keV. The instantaneous, 15–250 keV background rate varies between 80 and 110 counts s^{-1} in each cluster depending upon location in the orbit. This translates to 4.3–5.9 $\times$ 10^{-4} counts cm^{-2} s^{-1} keV^{-1} averaged over the full energy range.

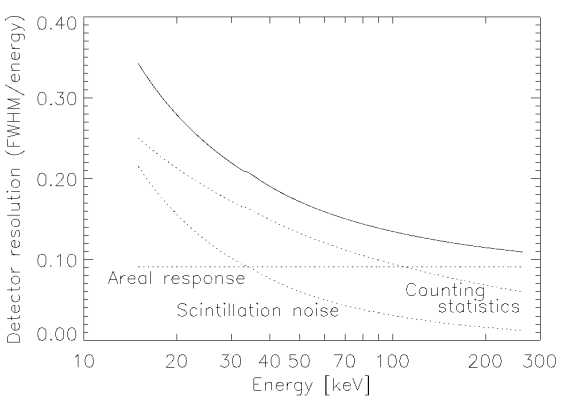

FIG. 4.—Energy resolution, $\Delta E/E$, as a function of energy, E, for one of the HEXTE detectors. The three components of the energy resolution are shown. The component labeled "Counting statistics" is due to the stochastic nature of the charge generation in the photomultiplier tube and has an $E^{-0.5}$ dependence. The constant factor labeled "Areal response" reflects the variation of light collection efficiency across the detector. Finally, the additional width due to long-lived states in the NaI(Tl) stimulated by cosmic rays contributes proportionally to E^{-1}, and is labeled "Scintillation noise." The small bump at 33 keV results from the lower light output of NaI(Tl) for events just above the K edge of iodine due to the lower energy of the photoelectron.

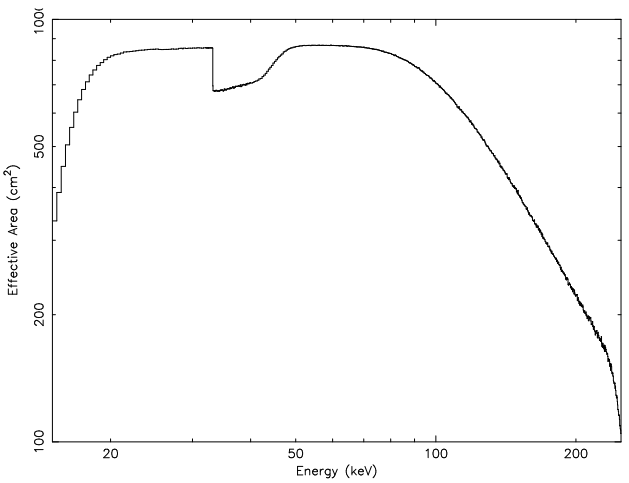

FIG. 5.—HEXTE effective area versus energy for cluster A. The reduction at lower energies is due to photoelectric absorption in the housing above the detector, while the reduction at higher energies is due to the finite NaI(Tl) thickness. The sharp drop and smooth recovery near 30 keV is due to the change in photoelectric cross section at the K edge of iodine and the onset of K-escape losses.

3.2. *Orbital Environment*

The *RXTE* orbit of 580 km altitude and 23° inclination results in the satellite passing through the trapped radiation of the South Atlantic Anomaly (SAA) for about one-half of

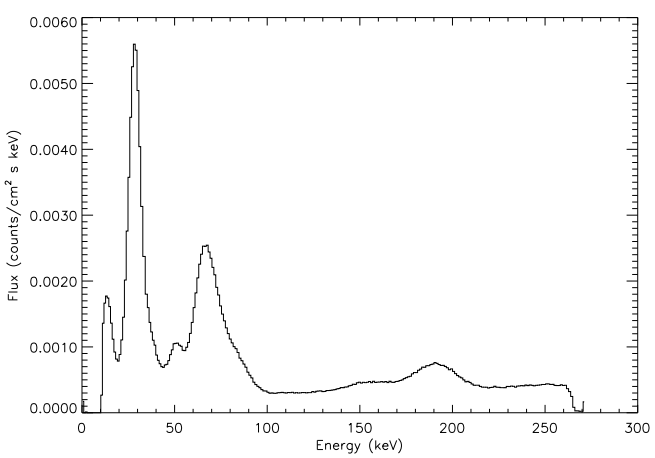

FIG. 6.—HEXTE background for a single detector plotted versus energy. Background lines due to activation of the iodine by cosmic and trapped radiation are evident at 30, 55, 66, and $\sim$190 keV, as are the $K_{\alpha\beta}$ lines at 74 and 85 keV from fluorescence of the lead collimator. The data are from a 7.5 hr observation of blank sky fields.

the orbits in a day and sampling a range of geomagnetic latitude throughout the day. Figure 7 shows typical counting rates from one HEXTE detector over a day. The lower level discriminator (LLD) rate is the total counting rate in the scintillators above 12 keV. Modulation of the charged particle flux due to varying geomagnetic rigidity cutoff is apparent in the non-SAA orbits between hours 3 and 13. Shutdown of the detectors during SAA passages and the subsequent 25 minute half-life radioactive decay of ^{128}I upon exit of the SAA are evident between hours 13 and 24. The upper level discriminator (ULD) rates reflect the total counting rate in the scintillators above 250 keV and are similar to the LLD rates apart from normalization. The extreme upper level discriminator (XULD) rate monitors events leaving more than 20 MeV in the crystals. This rate is dominated by interactions of energetic cosmic rays and exhibits modulation in the non-SAA orbits. Typical counting rates for the particle monitor (which are dominated by trapped radiation of the SAA) are also shown in Figure 7.

3.3. *Background Subtraction*

Since the HEXTE counting rate exhibits temporal variations in any given orbit, as seen in Figure 7, one must make a near real-time estimate of the background utilizing the source chopping system described above. This method's ability to provide accurate background subtraction is essential to HEXTE sensitivity.

One test of the background subtraction is to compare net rates to zero when viewing blank fields. The blank sky observations of 1996 January 15 covered 19 different pointing directions determined to be source free (flux <2 PCA counts s^{-1} assuming a power-law index of 1.7) from the *ROSAT* WGACAT (White, Giommi, Angellini catalog; White, Giommi, & Angellini 1994). These observations averaged ~ 10 minutes each. Figure 8 shows the background-subtracted rates in four energy bands (16–30, 31–60, 61–100, and 101–240 keV) for each cluster for each pointing direction. An average net rate and uncertainty was calculated for each rate and the χ^2 calculated for comparison to the average net rate. Table 3 gives these values along with the probability of exceeding χ^2 by a random fluctuation. In all cases the probability was less than 8%, indicating that the background-subtraction method used by HEXTE is quite effective for short observations.

Another test is to compare the spectra of the two off-source positions in a long observation that experiences a variety of orbital conditions. In 1996 January a 200 ks observation of MCG +8-11-11 was performed (see below) with 1°.5 offsets and 32 s dwell times. Background data from each off-source position were accumulated for both clusters. Subtraction of one blank sky off-source region from another provides a measure of the accuracy of this technique for long observations, where it is most important. The 200 ks observation resulted in 46 ks of on-source live time for each cluster (92.5 ks of 800 cm^2 total) and 40 ks at each off-source position for each cluster (80.6 ks of 800 cm^2 total). The net flux from these two off-source, blank sky positions is shown in Figure 9. Binned every five pulse-height channels, fluctuations from bin to bin are $\lesssim 1\%$ of background, and the broadband average is $(0.11 \pm 0.10)\%$, $(-0.34 \pm 0.10)\%$, and $(-0.11 \pm 0.07)\%$ for cluster A, cluster B, and their sum, respectively. At 100 keV the background is 3×10^{-4} counts cm^{-2} s^{-1} keV^{-1}. For equal on- and off-source viewing times of 10^5 s, this implies a 3 σ minimum detection sensitivity in a 20 keV band at 100 keV

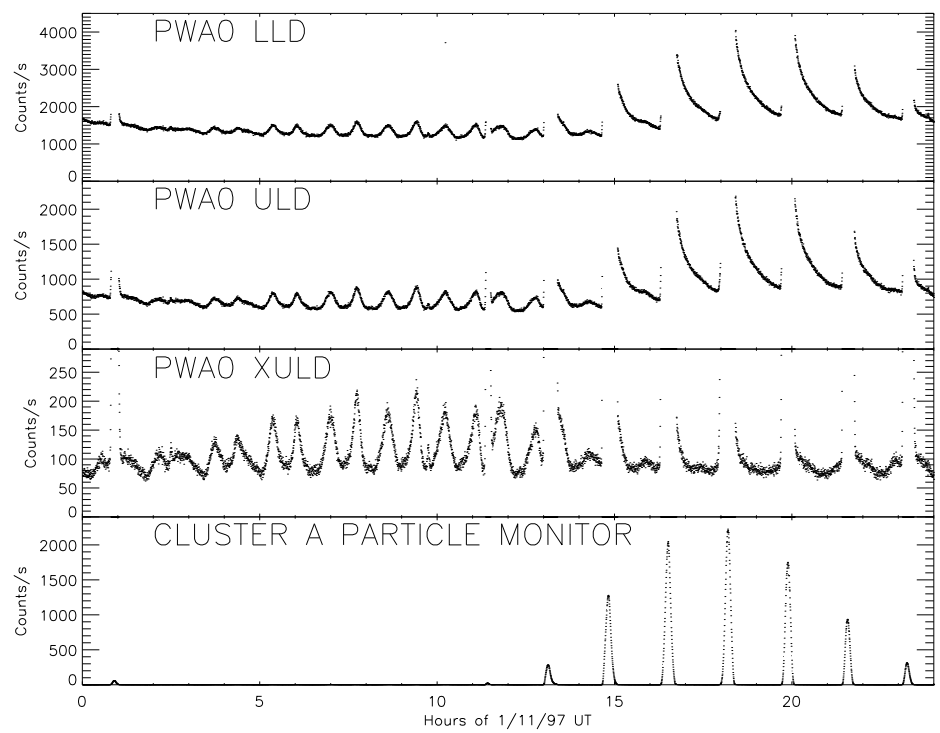

FIG. 7.—Counting rates from one HEXTE detector (Phoswich 0 in cluster A) for 1997 January 11. The rates from the phoswich detector are the lower level discriminator (LLD, events with energy losses >12 keV), upper level discriminator (ULD, events with energy loss >250 keV), and extreme upper level discriminator (XULD, events with energy loss >20 MeV). The fourth panel shows the particle monitor rate (charged particles with >0.5 MeV energy loss), which experiences large increases when transiting the SAA.

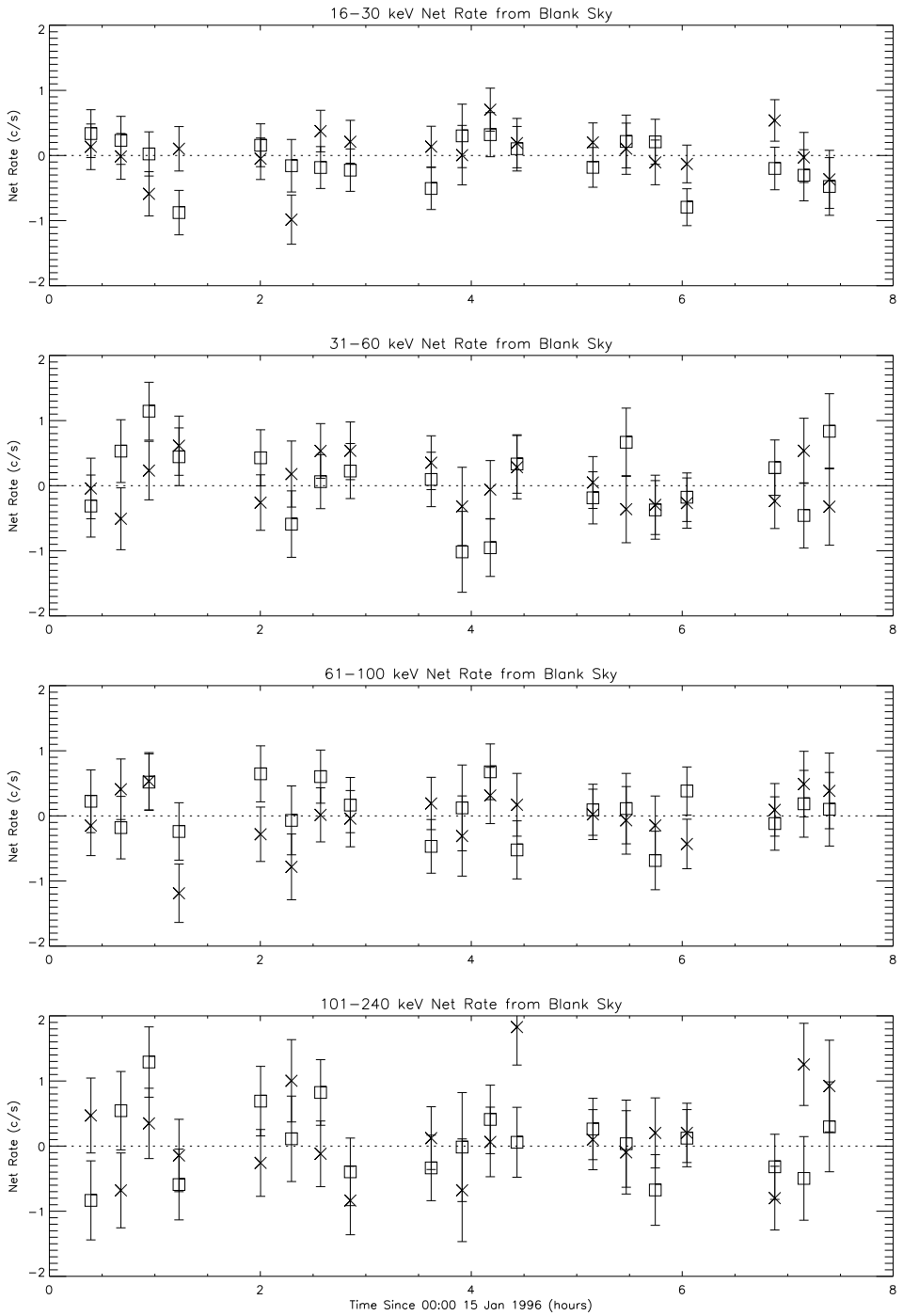

FIG. 8.—Background-subtracted counting rates for 19 observations (of 10 minutes each) of blank fields on 1996 January 15. The four sets of rates cover the energy range 16–30, 31–60, 61–100, and 101–240 keV. *Crosses*, cluster A; *squares*, cluster B; *dotted line*, zero net flux.

of 3×10^{-6} photons cm^{-2} s^{-1} keV^{-1}, or 1% of background (Gruber et al. 1996). This shows that the HEXTE background measurement technique is extremely effective for typical, long, weak source observations.

Finally, analysis of the background level as a function of aperture viewing direction for all observations of 50 ks or more is part of a doctoral thesis at UCSD on the diffuse background. This has led to a spectrum of the difference between the two off-source viewing directions (Fig. 10) accumulated over more than 5×10^6 s. (The on-source data are not available to us due to the proprietary nature of the observations.) The largest, single channel deviation is $\leq 1\%$ of the background rate in that channel (MacDonald et al. 1996). The 15–240 keV net rates in clusters A and B are $(-0.2 \pm 1.5) \times 10^{-3}$ and $(0.5 \pm 1.2) \times 10^{-3}$ counts s^{-1}. The χ^2 fit of the 15–240 keV data to these averages was 211.0 and 215.1 for 224 degrees of freedom, respectively. This establishes that long-term integrations with HEXTE have systematic spectral uncertainties at a few tenths of a percent of background.

3.4. *Spectral Calibration*

Using the HEXTE effective area, which includes our present best estimate of the calibration parameters, we have

TABLE 3

χ^2 VALUES FOR FITTING BLANK SKY RATES

Energy Band	Cluster	Net Rate (counts s^{-1})	χ^2	χ^2/18 (dof)	Probability
15–30 keV	A	0.023 ± 0.081	20.91	1.16	0.284
	B	-0.106 ± 0.083	21.06	1.17	0.286
31–60 keV	A	0.034 ± 0.108	11.14	0.62	0.888
	B	0.052 ± 0.107	25.64	1.42	0.108
61–100 keV	A	-0.041 ± 0.106	16.05	0.89	0.589
	B	0.082 ± 0.108	14.82	0.82	0.674
101–240 keV.....	A	0.153 ± 0.197	26.72	1.48	0.084
	B	0.052 ± 0.133	18.47	1.03	0.425

fitted the total, dead-time corrected, Crab Nebula/pulsar spectral data from each HEXTE cluster in the 15–240 keV range. The best-fit photon index for a single power law was $\Gamma = 2.062 \pm 0.001$ with a normalization at 1 keV of 6.73 ± 0.02 photons cm^{-2} s^{-1} keV^{-1}. The ratio of this normalization between clusters A and B was 1.023. This observed index is somewhat flatter than those seen by other instruments (Bartlett 1994, and references therein). Since the spectrum is known to steepen near 100 keV (Jung 1989), the value of an effective average index is dependent on the energy range over which the fit is attempted. Accordingly, the HEXTE data were fitted to a power law that breaks sharply at a single energy to a second power law (i.e., a broken power-law model). In this case the photon index below the break energy was found to be $\Gamma_1 = 2.045 \pm 0.002$, the break energy was $E_B = 57.2 \pm 3.0$ keV, and the photon index above the break energy was $\Gamma_2 = 2.140 \pm 0.009$. The χ^2 was reduced by 210 for 433 degrees of freedom in going from the single power law to the broken power law. The reduced χ^2 for the latter was 1.80. The instrument counts histogram and best-fit broken power-law model are shown in Figure 11 along with the ratio of the data to the model. The higher energy data have been rebinned into 10 keV groups for display only—the fitting was done to 219 pulse-height channels in each cluster.

The broken power-law fits can be compared to Barlett (1994), who reported $\Gamma_1 = 2.00 \pm 0.03$, $E_B = 60 \pm 7$ keV, and $\Gamma_2 = 2.22 \pm 0.03$, and to Jung (1989) with $\Gamma_1 = 2.075 \pm 0.005$, $E_B = 127.7 \pm 3.6$ keV, and $\Gamma_2 = 2.48 \pm 0.03$. The HEXTE broken power-law normalization at 1 keV was 6.38 ± 0.03 photons cm^{-2} s^{-1} keV^{-1}, which is less than that seen for *HEAO 1* (8.76 ± 0.03 photons cm^{-2} s^{-1} keV^{-1}; Jung 1989) in the 17–2300 keV range. The majority of this normalization discrepancy, we believe, is in the assumed shape of the collimator response near its peak. A perfect, pointed peak is assumed presently. The more accurate collimator shape is being calculated from multiple scans across the Crab, and will be the basis for a revision in the HEXTE open area calculation in the near future. We have found minimal energy dependence to the normalization ($\Gamma_1 = 2.050 \pm 0.002$ and 2.037 ± 0.003 for clusters A and B respectively), and thus, fitting with a normalization parameter as part of the fitting procedure for other sources is warranted. These details are the subject of continuing calibration efforts with the PCA and HEXTE instrument teams. The differences between the HEXTE fitted values and those from *HEAO 1* and the GSFC balloon instrument reflect the present HEXTE systematic uncertainties, those of those past missions, and the fact that a broken power law is too simple of a model for the spectral evolution in the Crab total spectrum.

3.5. *Absolute Timing*

The HEXTE timing information, as well as that of *RXTE*, was verified through observations of the Crab pulsar. The arrival time of each photon was corrected to the solar system barycenter and folded using the Crab pulsar radio ephemeris appropriate to that time. Figure 12 shows the light curves for the entire HEXTE 15–250 keV energy range and for three energy intervals within the HEXTE range. The pulse profile consists of two sharp peaks separated by 0.4 in phase but connected by a "bridge" of pulsed emission. The sharp pulsed components plus the bridge, or interpulse, connecting them are as expected from previous observations (e.g. Ulmer et al. 1994). Zero phase is defined as the center of the first peak in the radio with the ephemeris parameters given in Table 4. For this observation the first peak is within one phase bin (300 μs) of the radio peak, and thus the HEXTE absolute time reference is accurate within a fraction of a millisecond. From the plot it is apparent that the second peak in the folded light curve has a harder spectrum than the first peak, as indicated by its increasing dominance over the first peak with increasing energy.

3.6. *Response to High Rates*

Three weeks after launch, *RXTE* began a series of target of opportunity observations of the bursting pulsar, GRO J1744−28. At this time the source's 2–10 keV flux was about twice that of the Crab with bursts up to a factor of 10 brighter lasting for about 10 s. The HEXTE was designed to handle persistent rates as high as 5 times that of the Crab, and to recover quickly from rates in excess of that. The bursts from GRO 1744−28 clearly exceeded that rate. This is demonstrated in Figure 13 where the 2.1 Hz pulsations are seen before and after the less than 2 s of lost data at the peak of the burst. HEXTE lost data at the peak of the counting rate due to a finite number of data buffers, and the data transmission resumed once buffers again became available.

3.7. *Hard X-Ray Spectrum of a Weak Source (MCG +8-11-11)*

The Seyfert 1 active galaxy MCG +8-11-11 was observed over the period from 1996 January 7–29 to verify

TABLE 4

CRAB PULSAR EPHEMERIS

Characteristic	Value
f (Hz).....	29.8861513101
$\dot{f}$ (Hz^2).....	-3.75733×10^{-10}
T_0 (MJD).....	50,311.000000119
R.A.....	83°.633121
Decl.....	22°.014460

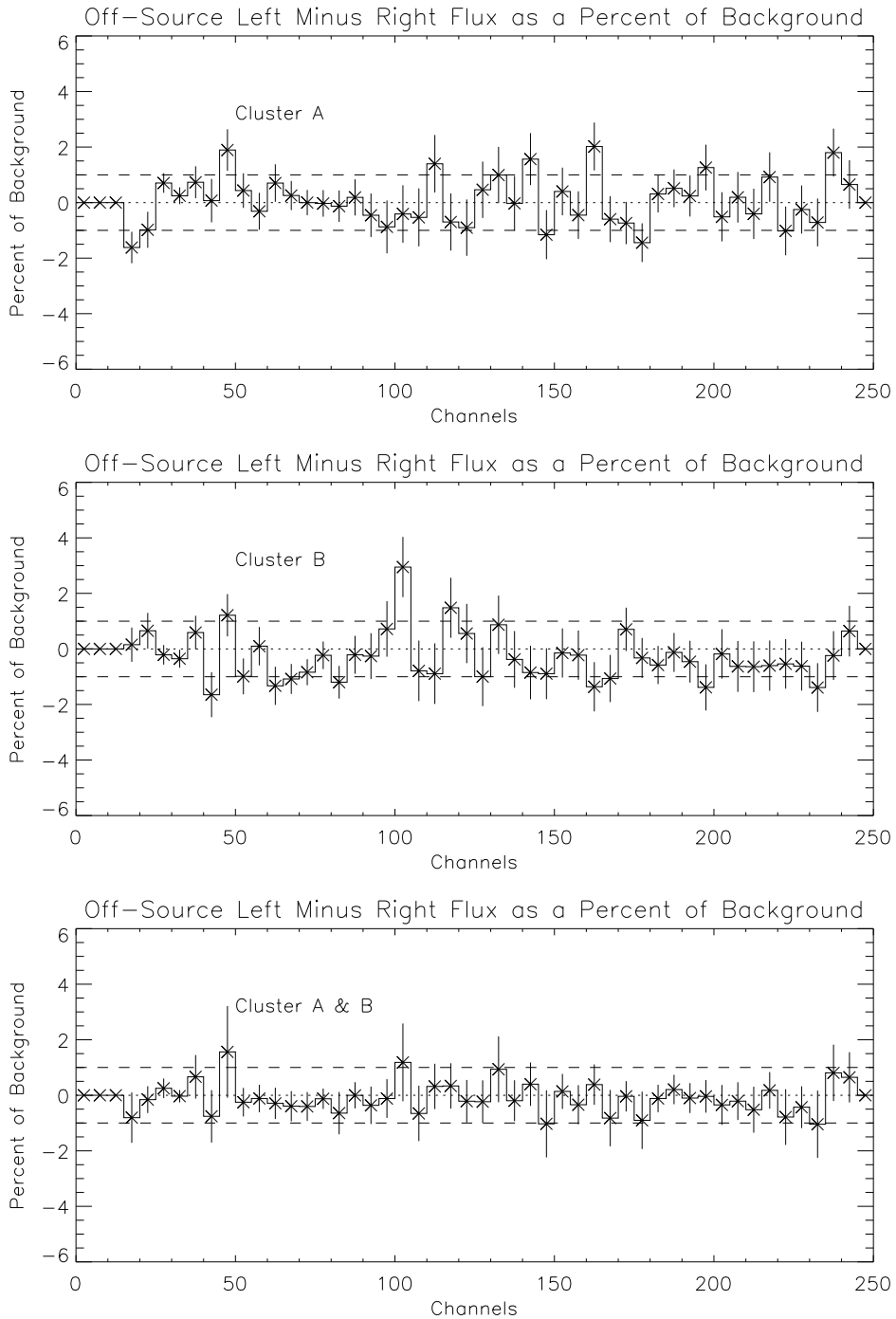

FIG. 9.—Net counting rate histogram of the difference of the two off-source positions for each cluster and their sum during the MCG +8-11-11 observation. One percent of the total off-source flux is shown by pairs of horizontal dashed lines for comparison. "Left" and "Right" correspond to the plus and minus directions of the off-source viewing.

the overall performance of HEXTE when observing a weak source. Basic results on the 15–240 keV HEXTE spectrum of MCG +8-11-11 are presented to demonstrate the HEXTE capabilities for spectral studies of weak sources, such as active galaxies. Further analysis and interpretation of MCG +8-11-11 results will be the topic of a future paper.

This source has been observed in the 0.5–20 keV range over the last 25 years (Elvis et al. 1978; Mushotzky et al. 1980; Petre et al. 1984; Turner & Pounds 1989; Treves et al. 1990; Grandi et al. 1998) to be a simple power law ($\Gamma \approx 1.7$) modified by low-energy absorption ($N_{\rm H} \approx 2.5 \times 10^{21}$ cm^{-2}). At higher energies, the OSSE measurement (Johnson et al. 1997) found a steeper index ($\Gamma = 2.7 \pm 0.4$) in the energy range 50–150 keV, and the Milan/Southhampton Collaboration (MISO) balloon instrument (Perotti et al. 1981) found a flatter ($\Gamma = 1.0 \pm 0.7$) index from 20 keV to 1 MeV.

The HEXTE measurement contains 92.6 ks of 800 cm^2 exposure on source and 80.6 ks off source. Fitting with a single power law yields a best fit for the index of $\Gamma = 2.18 \pm 0.09$ with 20–50 keV flux of $2.70 \pm 0.11 \times 10^{-11}$ ergs cm^{-2} s^{-1} and is shown in Figure

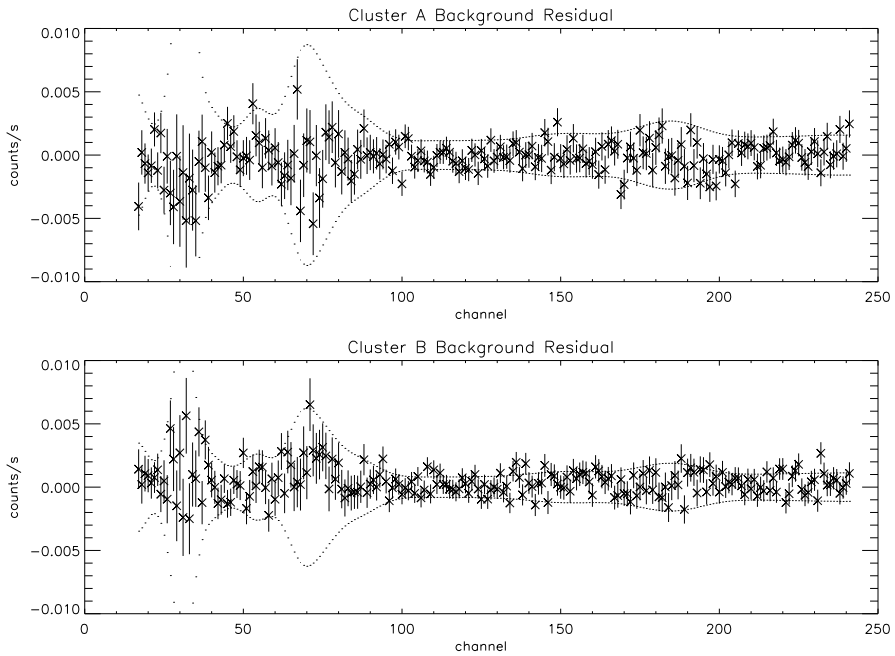

FIG. 10.—Net off-source counting rate histogram versus pulse-height channel for a 5×10^6 s accumulation of observations with greater than 50 ks duration for the two HEXTE clusters. The detector gain is approximately 1 keV per channel, and the energy range covered is 15–240 keV. The dotted lines represent $\pm 0.5\%$ of the background per channel.

14. The χ_ν^2 was 1.14 for 221 degrees of freedom (the data from the two clusters were combined before fitting). The best-fit index is intermediate between the lower energy index (~ 1.7) and the higher energy value (2.7 ± 0.4) mentioned above. This is indicative of a more complex spectrum with a break at higher energies. Indeed, Grandi et al. (1998) have suggested that a reflection component in conjunction with a cutoff power law ($\Gamma = 1.73 \pm 0.06$, $E_C = 266^{+90}_{-68}$) may be a better representation of the MCG +8-11-11 spectrum from analysis of concurrent *ASCA* and OSSE data taken 4.5 months before the *RXTE* observation. Using a cutoff power law, the HEXTE values are $\Gamma = 1.90 \pm 0.35$, $E_C = 120.8 \pm 120.8$ with a reduced χ^2 of 1.17. The HEXTE results are consistent with the *ASCA*/OSSE values.

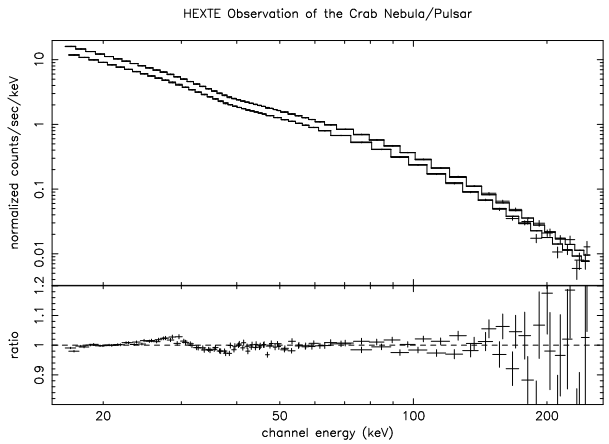

FIG. 11.—HEXTE counts histogram versus energy plus best-fit broken power-law model for fitting the Crab Nebula/pulsar spectrum in clusters A and B simultaneously. The upper plot shows the observed data plus model for each cluster with higher energy data rebinned into 10 keV groups for display only. The lower plot shows the ratio of the residuals of the best-fit model to the data.

4. CONCLUSIONS

Since its launch at the end of 1995, the HEXTE has performed extremely well, with the one exception of the increased dead time needed for recovery after large energy deposits in the crystals. The tight control of systematics allows for measurements of weak sources to better than 1% of background and for absolute timing at the submillisecond level. HEXTE observations of the Seyfert galaxy MCG +8-11-11 show that *RXTE* can extract the source spectrum of weak active galacitc nuclei to 100 keV or more in 200 ks observations. Observations of the Crab Nebula and pulsar verified the *RXTE* absolute timing to significantly less than a millisecond, and detected the break in the total Crab spectrum near 60 keV. These examples confirm that users can expect to extract details of spectral components that will lead to a better understanding of the processes and geometries of X-ray sources using *RXTE*.

The HEXTE team would like to acknowledge the guidance of Laurence Peterson in the development of HEXTE, the technical advice of James Matteson, and the support of the *RXTE* mission by Alan Bunner, Louis Kaluzienski, and others at NASA Headquarters over the decade and a half from proposals to launch. The HEXTE development depended upon the expertise and dedication of an exceptional technical and programmatic staff, including Edwin Stephan Jr., Robert Howe, Shirley Roy, Fred Duttweiler, Phillipe Leblanc, Charles James, George Huszar, Tom Gasaway, Richard Bentley, Mathew Marlowe, Shalom Halevy, Trevor Lillie, Georgia Hoopes, Ginger Beriones, and Paul Yeatman. We thank the Scripps Marine Machine shop and Jack Kuttner.

We acknowledge the excellent work developing the HEXTE flight electronics and flight software of the Perkin Elmer Applied Science Division (now a division of Orbital Sciences Corporation) under the management of Robert Kobiyashi and Robert Hertel.

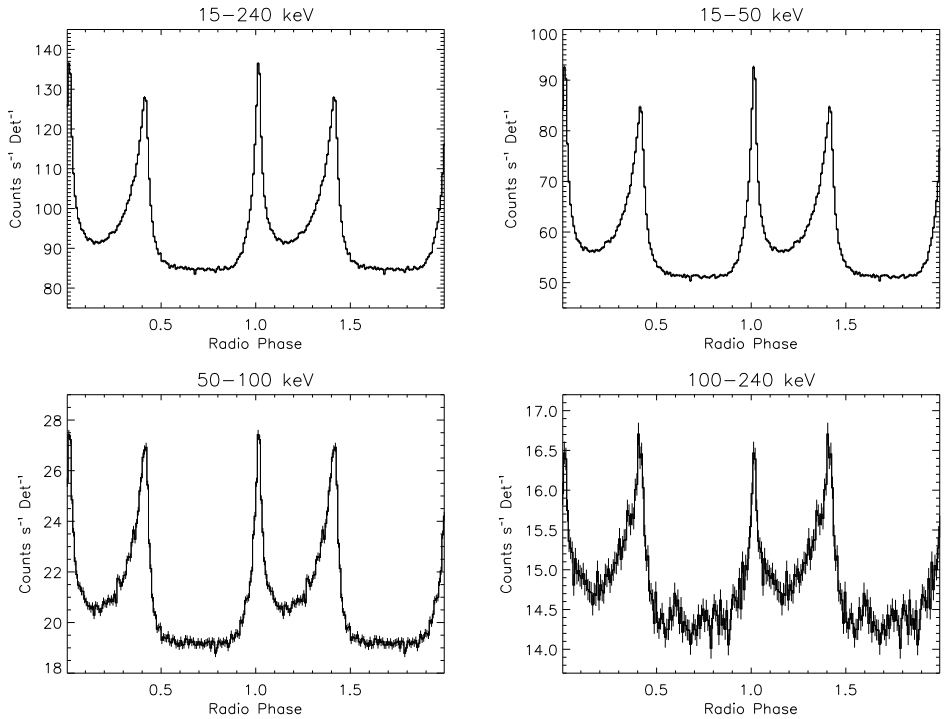

FIG. 12.—Folded light curves of the Crab Nebula and pulsar based upon the radio ephemeris. Light curves are shown for the entire 15–250 keV HEXTE energy range and for the energy ranges 15–50 keV, 50–100 keV, and 100–240 keV. The X-ray to radio offset is less than 1 ms.

We also would like to thank the Goddard Space Flight Center spacecraft engineers for providing us with a superb, flexible, and intelligent spacecraft that has met and exceeded all our expectations. We acknowledge the hard work and determination of the *XTE* Project office through the many evolutions of the spacecraft and launch vehicle concepts. Dale Schulz and the rest of the project team are to be congratulated. We thank our colleagues on the instrument teams at GSFC and MIT, and the *XTE* Science Working Group for excellent discussions of technical and programmatic problems over the years. Finally, we thank the late Leon Herried for the software concept to operate the *RXTE* in a flexible and straightforward manner. We also thank the anonymous referee for suggesting improvements to the paper. This work was supported by NASA contract NAS5-30720.

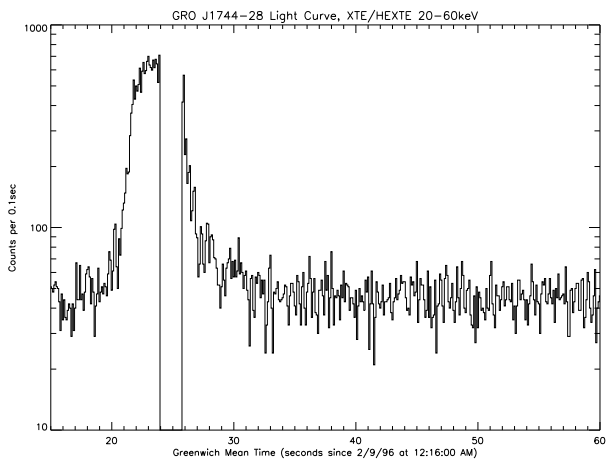

FIG. 13.—Light curve of the bursting pulsar 1744−28 taken during the in-orbit checkout phase of the *RXTE* mission. Individual pulses at the 2.1 Hz pulse period are evident in the persistent flux and a burst is also evident. The less than 2 s dropout and recovery of data during the burst were caused when X-ray rates exceeded the maximum transferable rate.

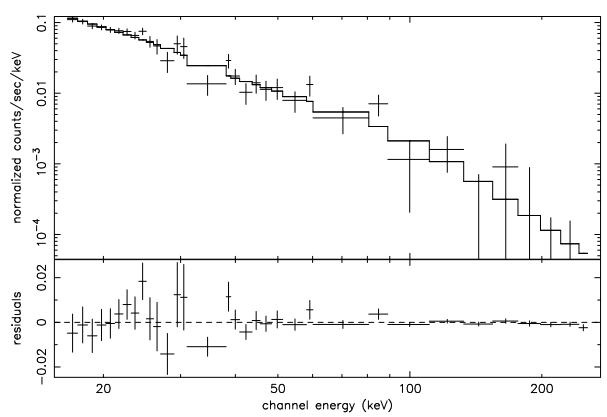

FIG. 14.—Oserved HEXTE counts histogram from MCG +8-11-11 compared to the best-fit power-law model. The HEXTE data at higher energies have been rebinned for display only into ~20 keV bins. The lower panel displays the residuals of the observed counts to the predicted best-fit model counts.

REFERENCES

Bartlett, L. M. 1994, Ph.D. thesis, University of Maryland
Elvis, M., Maccacaro, T., Wilson, A. S., Ward, M. J., Penston, M. V., Fosbury, R. A. E., & Perola, G. C. 1978, MNRAS, 183, 129
Grandi, P. Haardt, F., Ghisellini, G., Grove, E. J., Maraschi, L., & Urry, C. M. 1998, ApJ, submitted
Gruber, D. E., Blanco, P. R., Heindl, W. A., Pelling, M. P., Rothschild, R. E., & Hink, P. L. 1996, A&AS, 120, 641
Hink, P., Pelling, P., & Rothschild, R. 1992, Proc. SPIE, 1743, 140
Hink, P. L., Rothschild, R. E., Pelling, M. R., MacDonald, D. R., & Gruber, D. E. 1991, Proc. SPIE, 1549, 193
Jahoda, K., et al. 1996, Proc. SPIE, 2808, 5
Johnson, W. N., et al. 1997, 4th Compton Symposium, ed. C. D. Dermer, M. S. Strickman, & J. D. Kurfess (Woodbury: AIP), 283
Jung, G. V. 1989, ApJ, 338, 972
Levine, A. M., et al. 1996, ApJ, 469, L33
MacDonald, D. R., et al. 1996, BAAS, 28, 1316
Mushotzky, R. F., Marshall, F. E., Boldt, E. A., Holt, S. S., & Serlemitsos, P. J. 1980, ApJ, 235, 377
Pelling, M. R., Rothschild, R. E., MacDonald, D. R., Hertel, R., & Nishiie, E. 1991, Proc. SPIE, 549, 134
Perotti, F., Della Ventura, A., Villa, G., Di Cocco, G., Butler, R. C., Carter, J. N., & Dean, A. J. 1981, Nature, 292, 133
Petre, R., Mushotzky, R. F., Krolik, J. H., & Holt, S. S. 1984, ApJ, 280, 499
Rothschild, R. E., Pelling, M. R., & Hink, P. L. 1991, Proc. SPIE, 1549, 120
Swank, J. H., et al. 1995, The Lives of the Neutron Stars, ed. M. A. Alpar et al. (Dordrecht: Kluwer), 525
Treves, A., Bonelli, G., Chiappetti, L., Falomo, R., Maraschi, L., Tagliaferri, G., & Tanzi, E. G. 1990, ApJ, 359, 98
Turner, T. J., & Pounds, K. A. 1989, MNRAS, 240, 833
Ulmer, M. P., et al. 1994, ApJ, 432, 228
Wayne, L. R., Heindl, W. A., Hink, P. L., & Rothschild, R. E. 1998, Nucl. Instrum. Methods Phys. Res., in press
White, N. E., Giommi, P., & Angelini, L. 1994, IAU Circ. 6100